Peer-reviewed version available at *Materials* **2017**, *10*, 591; doi:10.3390/ma10060591

Ultrathin Six-Band Polarization-Insensitive Terahertz Perfect Metamaterial Absorber Based on a Cross-Cave Patch Resonator

Yong Zhi Cheng[1*], Mu Lin Huang[1], Hao Ran Chen[1], Zhen Zhong Guo[2], Xue Song Mao[1], and Rong Zhou Gong[3]

[1]School of Information Science and Engineering, Wuhan University of Science and Technology, 430081, People's Republic of China
[2]Hubei Province Key Laboratory of Occupational Hazard Identification and Control, Wuhan University of Science and Technology;
[3]School of Optical and Electronic Information, Huazhong University of Science and Technology, Wuhan 430074, China

ABSTRACT: A simple design of an ultrathin six-band polarization-insensitive terahertz perfect metamaterial absorber (PMMA) composed of a metal cross-cave-patch resonator (CCPR) placed over a ground plane was proposed and investigated numerically. The numerical simulation results demonstrate that the average absorption peaks are up to 95% at six resonance frequencies with high quality-factors (>65). In addition, the absorption properties can be kept stability for both normal incident transverse magnetic (TM) and transverse electric (TE) waves. The physical mechanism behind the observed high level absorption is illustrated by the electric and power loss density distributions. The different absorption mainly originates from the higher order multipolar and multipolar plasmon resonance of the structure, which are sharp different to the most previous studies of the PMMAs. Furthermore, the resonance absorption of the PMMA can be tunable by varying the geometric parameters of the unit cell.

Key words: Perfect metamaterial absorber, terahertz, six-band, cave-cross patch resonator

1 Introduction

*Corresponding author: Yong Zhi Cheng (chengyz@wust.edu.cn,cyz0715@126.com)

Since the perfect metamaterial absorber (PMMA) concept was firstly proposed and demonstrated experimentally by Landy et al. [1], which has been become a hot research topic of science and technology. PMMAs have recently been developed rapidly in a wide electromagnetic (EM) spectrum range from microwave [1-3], terahertz [4-11], infrared [12-16], to visible region [17-20]. PMMA is not limited by the quarter-wavelength thickness and also scaled to different EM spectrum due to its geometry scalability. PMMAs have been proposed and demonstrated across a wide range of the EM spectrum and hold great potential applications such as thermal imaging [12], sensors [16], solar cells [21], and thermal emitters [22] and so on. Typical PMMA consists of three functioned layers: patterned metallic structure (eg. split-ring, cut-wire, patch, ring, and so on) as the EM resonator, a dielectric or magnetic substrate as a middle spacer, and continuous metal film or metal wire as the ground layer. Generally, PMMA can achieve near unity absorption based on fundamental resonance of the EM resonator. By adjusting the shape, size, thickness, and properties of patterned metallic structure and dielectric spacer; the permittivity $\varepsilon_{eff}(\omega)$ and permeability $\mu_{eff}(\omega)$ of the MMs can be equivalent and thus an impedance matched to free space [1-9]. For this fundamental EM resonance, the electric response is from the excitation of the electric resonators by the external electric field [5-7]. The magnetic response is usually provided by pairing the top layer with a metal ground plane or metal wire for an external magnetic field of the normal incident EM waves. The strong local EM resonance also restricts the unique responses to only a single narrow band absorption, which greatly affects its applications, particularly for sensor, detector and bolometer applications. Thus, in many cases, multi-band or broadband PMMAs are also necessary.

Many efforts have been made to try to achieve multi-band or broadband high level absorption for EM wave [23-29]. Generally, there are two design strategies for PMMAs to achieve multiband absorption or extend the absorption bandwidth. The one approach is to combine multiple non-degenerate sub-units within a coplanar super-unit resonant structure [6-8], and the other way is to construct an alternating multiple patterned metallic and dielectric layers with different geometric parameters

Peer-reviewed version available at Materials 2017, 10, 591; doi:10.3390/ma10060591

stacked vertically [24-28]. However, both the design strategies for the proposed multi-band or broadband PMMAs will suffer from some disadvantages: Firstly, the super-unit resonant structure should be very complicated, and thus increasing the fabrication cost of the PMMAs. Secondly, there are many interactions between the sub-units and resulting in the increased angular dependence in practices. Near all the above mentioned designs are based on the overlapping of the fundamental resonance of the patterned metallic structure with different geometric parameters, and usually neglect the high-order EM response. In effect, high-order multipolar resonances of MMs are vital but often overlooked in the design of the multi-band PMMAs. It is very useful to design multi-band PMMA by combining the fundamental and high-order multipolar resonances in a single patterned metallic structure [3,8,11,30-32]. For example, Mao et al., demonstrate a multi-band PMMA based on Chinese ancient coin-shaped structures [3], which is attributed to the combination of the fundamental resonance (*LC* resonances) and dipole resonances. Dayal reported a multiband PMMA comprised of metallic circular gold micro-discs separated from a metallic thin film by a dielectric zinc sulphide film, and the multi-band perfect absorption originate from the excitation of multipole resonances at infrared wavelengths [30]. Dung et al., presented a broad PMMA and clarified that the mechanism of dual-band absorption is due to fundamental and third-order magnetic resonances [31]. Wang et al., proposed a PMMAs based on a single patched structure, which can achieve dual-band or trip-band absorption originated from the fundamental resonance and high-order resonance responses by appropriate geometric parameters design. However, most designs are focused on the dual-band and triple-band PMMAs, and some of which is polarization sensitive, the multi-band especially six-band PMMAs are rarely demonstrated [32].

In this paper, we present a simple design of the ultrathin six-band polarization-insensitive PMMA in terahertz region. Our design consists of an array of cross-cave patch resonator (CCPR) and a copper ground plane separated by a thin Gallium Arsenide (lossy) (GaAs) dielectric film. Six ultra-narrow absorption bands are obtained, and these resonance peaks are average larger than 95%. Compared with

the previous reported PMMAs [3-11, 25-28, 30-32], our design has some advantages: Firstly, our PMMA has a novel resonance mechanism and a compact unit size design. Secondly, the simple design of PMMA has more absorption peaks in a single patterned metallic structure, which also is polarization-insensitive for normal incident wave. Thirdly, the Q-factors of our design are much larger than those of previous PMMAs. Such a simple design may provide some potential applications in biological sensing, material detection, thermal imaging and communications at terahertz frequencies.

2 Structure Design and Simulation

We introduce a simple and compact unit cell for six-band PMMA, as shown in Fig. 1. The designed PMMA is composed of a metallic CCPR array above a ground plane layer separated by a dielectric substrate. Fig. 1(a) depicts a 2D array structure of the designed PMMA, and the front view and respective view of the unit cell are displayed in Figs. 1(b,c). The optimized geometrical parameters of the unit cell of the PMMA are as follows: $p_x = p_y = 75\mu m$, $l = 68\ \mu m$, $g = 1\ \mu m$, $t_s = 3.8\ \mu m$. In our interested frequency range (0.8-3.2 THz), the metal elements (CCPR array and ground plane layer) were made of a lossy copper film with a frequency independent conductivity $\sigma = 5.8\times10^7$ S/m and a thickness of 0.6μm, which is much larger than the typical skin depth in the Terahertz regime (to avoid transmission through the metallic film). The gallium arsenide (GaAs) with a complex dielectric constant of $\varepsilon = 12.9+0.0774i$ was selected as the dielectric spacer between two metallic layers.

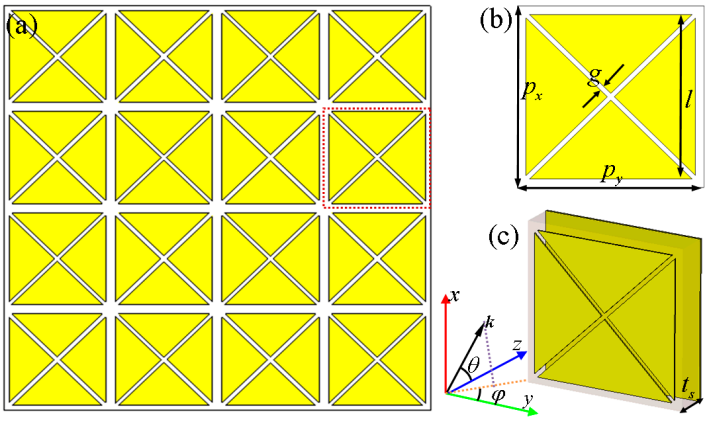

Fig.1. Schematic of the designed six-band PMMA: (a) 2D array, (b,c) front view and

respective view of the unit cell.

To verify the efficiency and investigate the resonant absorption behavior of our design, the full wave EM simulations were performed by using the frequency domain solver based on finite integration technology (FIT) in CST Microwave Studio. In the simulation, the periodic boundary conditions in the *x* and *y* directions are applied for the transverse boundaries to replicate an infinite array of the PMMA, and the perfectly matched layers are applied along the *z* direction. As shown in Fig.1(c), the periodic array structures are illuminated by a normally incident Terahertz plane wave with the electric field parallel to the *x*-axis. The absorbance of the designed PMMA can be defined as $A(\omega) = 1 - R(\omega) - T(\omega)$, where $A(\omega)$, $R(\omega)$, and $T(\omega)$ are the absorbance, reflectance, and transmittance as functions of frequency ω respectively. For plane wave normal incidence to our PMMA, there no transmission can be examined, as is blocked off by the continuous copper film. Thus, the $T(\omega) = 0$ and only the reflectance needs to be measured in our simulations. The absorptivity is possible to achieve unity ($A(\omega) \to 1$) when the reflection is near to zero ($R(\omega) \to 0$) at resonance frequency.

3 Results and Discussions

Figure 2 shows the simulated absorbance spectra of the proposed PMMA, there are six resonance frequencies (f_1, f_2… f_6) can be found. From Figs. 2(b-g), it can be clearly observed six absorption peaks at f_1 = 1.13 THz, f_2 = 1.56 THz, f_3 = 1.77 THz, f_4 = 2.18 THz, f_5 = 2.85 THz, and f_6 = 3.14 THz with absorbance $A(\omega)$ of about 90.5%, 94.4%, 98.7%, 96.2%, 95.4%, and 95.2%, respectively. The corresponding electric thickness of the PMMA is about $\lambda_1/70$, $\lambda_2/50$, $\lambda_3/45$, $\lambda_4/36$, $\lambda_5/28$, and $\lambda_6/25$, respectively (the λ_i is the resonance wavelength, where i = 1, 2, 3…6). Thus, our designed PMMA possess an ultra-thin thickness compared with the operation wavelength ($< \lambda/25$). In addition, it is also exhibited a frequency selectivity of the six-band PMMA due to the narrow bandwidth and the very small off-resonance absorption ($A(\omega) < 5\%$). The peak absorption at different frequencies is corresponding

to the nature of the different resonances modes, which will be further classified and illustrated by analyzing the distributions of the electric fields of the unit cell. It can be conjectured that the high level absorption of those six resonance peaks is attributed to the higher order multipolar plasmon resonances of the metallic square CCPR structure. It also can be found that the absorption band for six-peaks PMMA is relative narrow compared with the bandwidths of the previous PMMAs [5-8,11,12,32]. It is expected that the proposed PMMA has a significantly higher Q-factor than that of the previous ones.

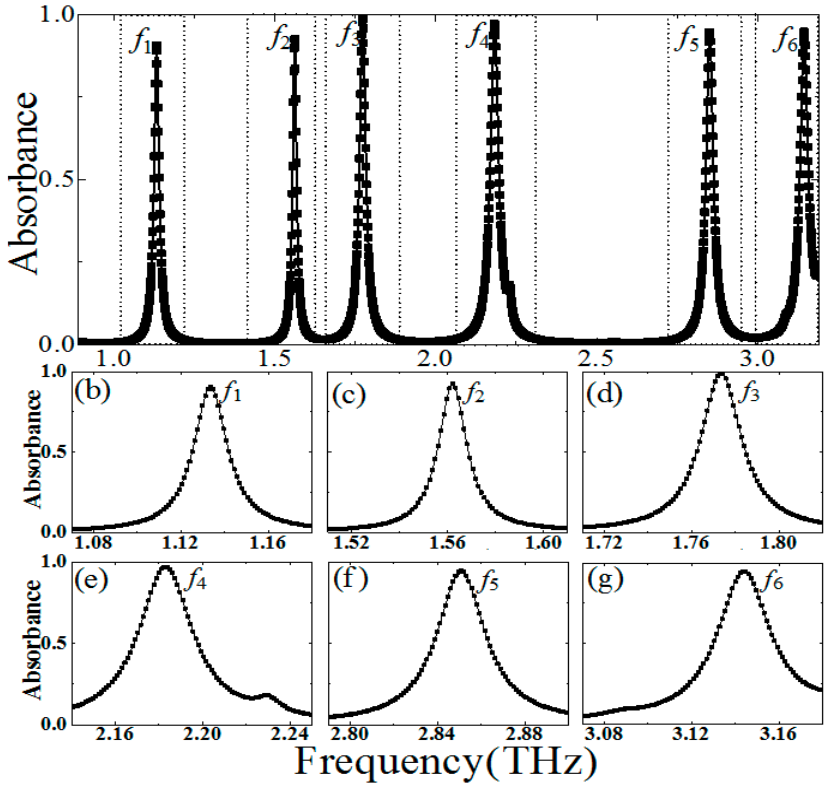

Fig.2. (a) The absorbance spectra of the proposed six-band PMMA, (b-g) the absorbance spectra under different resonance frequency domain.

The Q-factor is usually defined as the ratio of the central frequency to the full width at half maximum (FWHM) bandwidth of the resonance, which was calculated for our design. At above six resonance frequencies (f_1 = 1.13 THz, f_2 = 1.57 THz, f_3 = 1.77 THz, f_4 = 2.18 THz, f_5 = 2.83 THz, and f_6 = 3.14 THz), the FWHM bandwidths of the resonance is about 0.0167 THz, 0.0139 THz, 0.0219 THz, 0.0219 THz, 0.0251 THz, and 0.0286 THz, respectively. Thus, the corresponding Q-factor is about Q_1 =

Preprints (www.preprints.org) | NOT PEER-REVIEWED | Posted: 6 March 2017 doi:10.20944/preprints201703.0034.v1

Peer-reviewed version available at Materials 2017, 10, 591; doi:10.3390/ma10060591

67.48, Q_2 = 113.19, Q_3 = 80.6, Q_4 = 77.39, Q_5 = 112.67, and Q_6 = 109.53, respectively. From the above results, the high level absorption with higher Q-factor only occurs at resonance frequencies. That means this six-band PMMA has potential applications in sensor, detector and bolometer. In addition, it can be expected that the proposed structure of the PMMA is insensitive to polarization state of the incident terahertz wave due to the high symmetric of the structure.

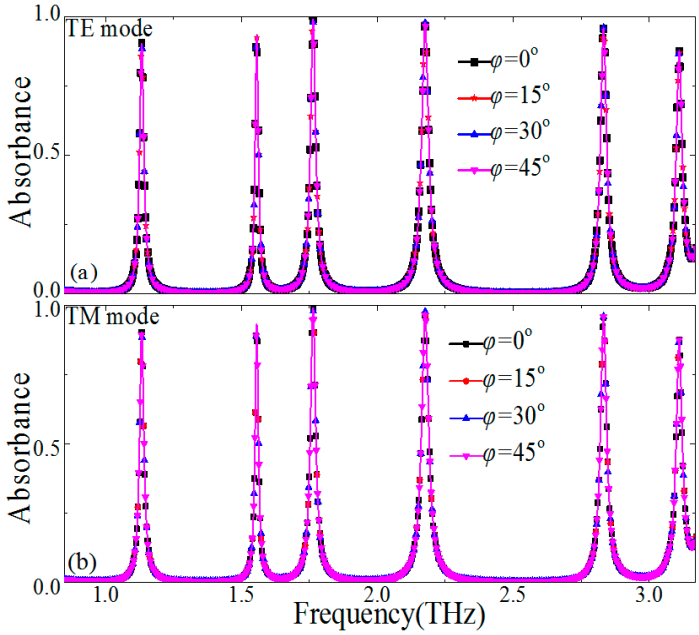

Fig. 3. Dependence of the absorption spectra on the polarization angles of the normal incident Terahertz wave for the proposed PMMA: (a) TE mode and (b) TM mode.

We characterize the polarization angles dependence of the PMMA for both TE and TM waves under normal incidence, and the results are shown in Fig. 3. We just need to consider the polarization angles from 0° to 45° owing to the high geometric symmetry of the unit cell structure of the PMMA, as shown in Figs. 3(a) and (b). Obviously, it can be seen that the absorbance under different polarization angles is nearly unchanging for both the TE and TM modes. It means that the designed PMMA can keep the absorption stability for normal incident terahertz waves with different polarization in practical application.

Peer-reviewed version available at Materials 2017, 10, 591; doi:10.3390/ma10060591

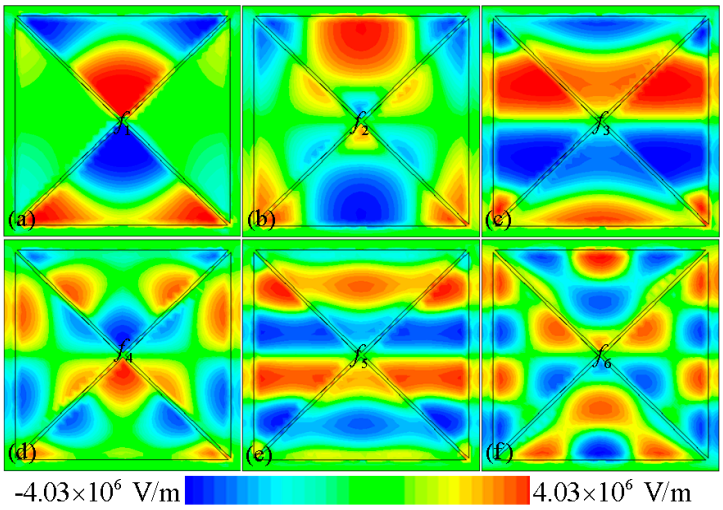

Fig.4. Distributions of z-component (E_z) of electric field for the proposed PMMA at frequencies of (a) f_1 = 1.13 THz, (b) f_2 = 1.56 THz, (c) f_3 = 1.77 THz, (d) f_4 = 2.18 THz, (e) f_5 = 2.85 THz, and (f) f_6 = 3.14 THz, respectively.

To illustrate the resonance absorption mechanism of the proposed PMMA, we calculated the electric field distributions for the six resonance frequencies, as shown in Fig. 4, which can give insight on the nature of the resonances. It can be observed that the z-component (E_z) of the electric field is mainly concentrated on the patch edges, gap edges, and corners of the metallic CCPR structure. As shown in the Fig. 4(a) for the lowest frequency f_1, the electric field is mainly concentrated on the corners of upper and lower triangle areas of the CCPR structure, indicating excitation of quadrupolar resonance in this structure. At the lowest resonance frequency (f_1), the upper and lower triangle areas of the resonator structure can strongly couple with the electric field and supply quadrupolar resonances, which also can be interpreted by a simple dipole–dipole interaction along the x-axis direction [33-36]. For the second resonance frequency f_2 as shown in Fig. 4(b), the upper and lower areas of CCPR structure and most part of the triangle section generate the half wave resonance mode, coupling strongly to the electric field. Similarly to the lowest mode (f_1), the CCPR structure at second mode (f_2) supplies hexapolar resonance. In effect, the electric field distributions revealing quadrupolar and hexapolar resonances correspond to natural of localized surface plasmon (LSP) behaviors [37]. From the Fig. 4(c) for the third resonance (f_3), the electric field distribution is concentrated on the upper, middle and

lower areas of the CCPR structure, which shows excitation of multiple half wavelength charge oscillations in the structure corresponding to the first higher order mode [30]. Essentially, the higher order modes occur at higher frequencies is due to the fact that the dimension of the CCPR structure is larger than a multiple of a half-wavelength of the resonance modes [8,11,30,32]. Similarly, as shown in Fig. 4(e), the electric field distribution at the fifth resonance mode (f_5) shows the next higher order excitation of multiple half wavelength charge oscillations in the CCPR structure. The electric field distributions for higher order mode possess a finite dipole moment for these two modes (f_3 and f_5), which is much like the fundamental dipole resonance response [30]. At the other resonance modes (f_4 and f_6) as shown in Figs. 4(d) the 4(f), the electric field distributions reveal decapole and octadecapole excitations of the CCPR structure [37]. It can be seen that the resonant electric fields associated with the multipolar modes (f_4 and f_6) are highly localized to the CCPR structure as well as highly enhanced in comparison to fields at nearby frequency. It should be noticed that the excitations of propagating surface plasmon also contribute to the formation of the absorption peaks (f_4 and f_6) [37]. This also means that the fourth and sixth absorption peaks (f_4 and f_6) originate from the combination of the high-order LSP and propagating surface plasmon resonance of the designed CCPR structure [37]. Therefore, this six-band PMMA is obtained based on the combination of the propagating surface plasmon resonance and high-order multipolar response of the CCPR structure. These results suggest a new approach to design a multi-band PMMA by integrating different resonance modes in a single patterned structure.

To further characterize the Terahertz wave resonance absorption behavior of the proposed six-band PMMA, we simulate the distributions of power loss density of the unit-cell structure, as shown in Figs. 5(a–f). It can be observed clearly that the regions of maximum power loss density mainly occur around the gap, upper and lower edges and other side areas of middle dielectric layer for the proposed PMMA. In effect, the majority of the Terahertz wave EM energy is dissipated as ohmic loss in the CCPR structure and dielectric loss in the middle dielectric layer at the different resonance modes. For example, as shown in Fig. 5(a), the distribution of power loss

density is mainly concentered on gap of the structure, which is induced by excitation of quadrupolar resonance. From the Figs. 5(b-f), it can be observed that the properties of power loss density distributions are similar to the electric field distributions. Obviously, the distributions of power loss density associated with the higher-order multipolar modes are highly localized to the CCPR structure. Thus, it can be concluded that the propagating surface plasmon resonance and high-order multipolar resonances play an important role for the high level absorption at the resonant frequencies.

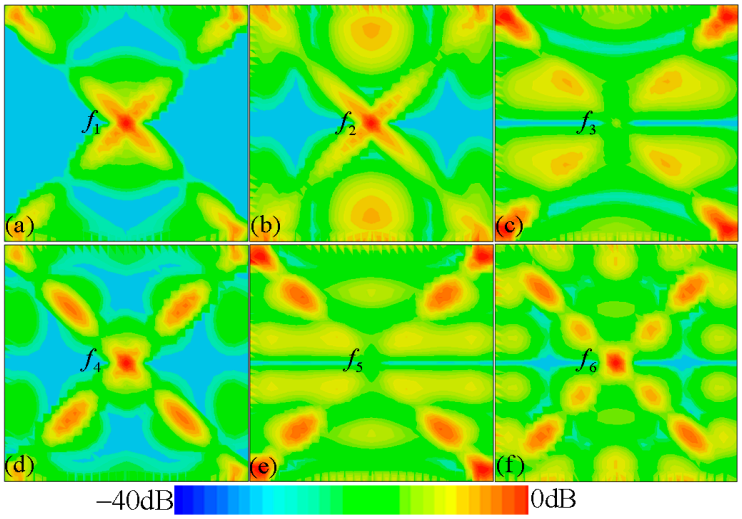

Fig.5. Distributions of power loss density in the middle dielectric layer for the proposed PMMA at frequencies of (a) 1.13 THz, (b) 1.56 THz, (c) 1.77 THz, (d) 2.18 THz, (e) 2.84 THz, and (f) 3.14 THz, respectively.

Based on the above explanations of the resonance absorption mechanism of the six-band PMMA, the influence of geometric parameters of the unit cell on the resonance frequencies can be easily understood. It can be conjectured that the frequencies of the PMMA mainly depend on the length l, gap width g of the metallic CCPR and the thickness t_s of the dielectric layer. Taking a further step, we study the geometric parameters of the unit cell on the resonance absorption properties of the PMMA.

Preprints (www.preprints.org) | NOT PEER-REVIEWED | Posted: 6 March 2017 doi:10.20944/preprints201703.0034.v1

Peer-reviewed version available at Materials 2017, 10, 591; doi:10.3390/ma10060591

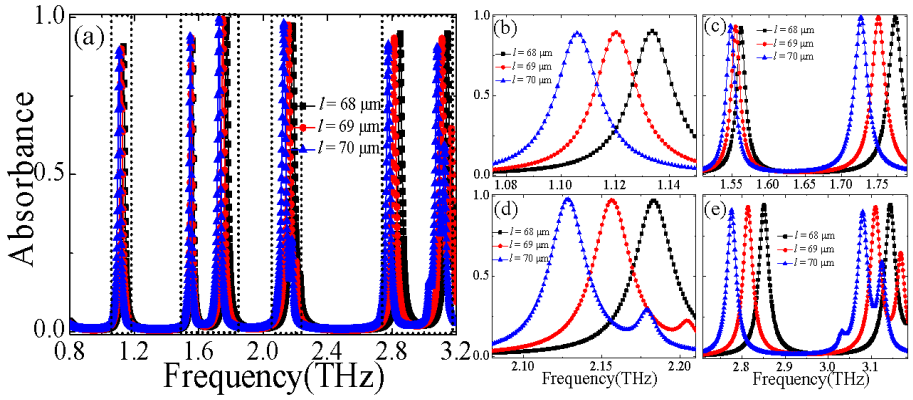

Fig.6. (a) Dependence of the absorption spectra of the proposed PMMA on the size changes of the CCPR length l (l = 68 μm, 69 μm, 70 μm), (b-e) the dependence of the absorbance spectra on the l under different frequency domain.

Firstly, the PMMA with different CCPR length l (l = 68 μm, 69 μm, 70 μm) were calculated with the other geometric parameters fixed, as shown in Fig.6. It can be observed that the CCPR length l change of the metallic CCPR array can influence the frequencies of the all resonance (f_1, f_2, f_3, f_4, f_5, and f_6), which will decrease with the increase of the CCPR length l. In addition, the absorption peaks of the resonance modes f_1, f_2, f_3, and f_4 will nearly unchanged, while the ones of the other resonances (f_5 and f_6) will increase with the increase of the CCPR length l.

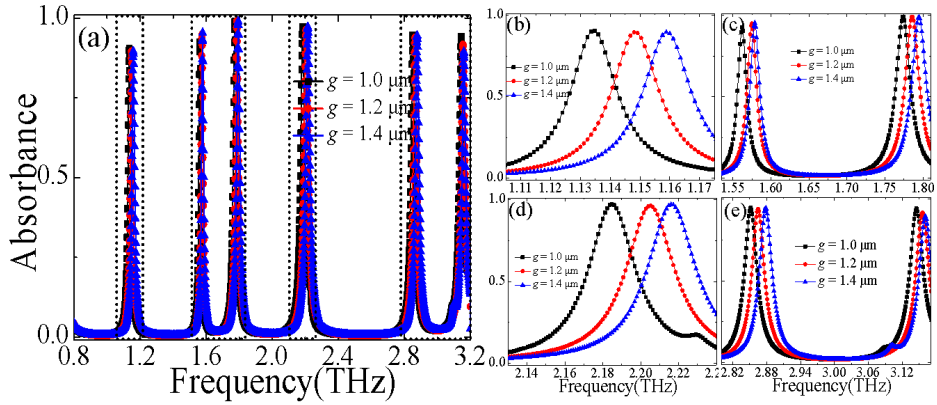

Fig.7. (a) Dependence of the absorption spectra of the proposed PMMA on the size changes of the CCPR gap width g (g = 1 μm, 1.2 μm, 1.4 μm), (b-e) the dependence of the absorbance spectra on the g under different frequency domain.

Next, we discuss the effect of CCPR gap width g on the absorption, and the absorbance of the PMMA with different CCPR gap width g (g = 1 μm, 1.2 μm, 1.4 μm)

Preprints (www.preprints.org) | NOT PEER-REVIEWED | Posted: 6 March 2017 doi:10.20944/preprints201703.0034.v1

Peer-reviewed version available at Materials 2017, 10, 591; doi:10.3390/ma10060591

have been calculated with the other geometric parameters unchanged, as shown in Fig.7. From the Figs.7 (b-e), it is seen that the resonance absorption frequencies (f_1, f_3, f_4, and f_5) drift to the higher frequency and the absorption peak remains unchanged with high level when changing the parameter g from 1 μm to 1.4 μm. Although the absorption frequencies (f_3 and f_6) also shift to the higher frequency, the absorption peak of modes f_3 will increase while the one of the modes f_6 will decrease with the increase of the CCPR gap width g.

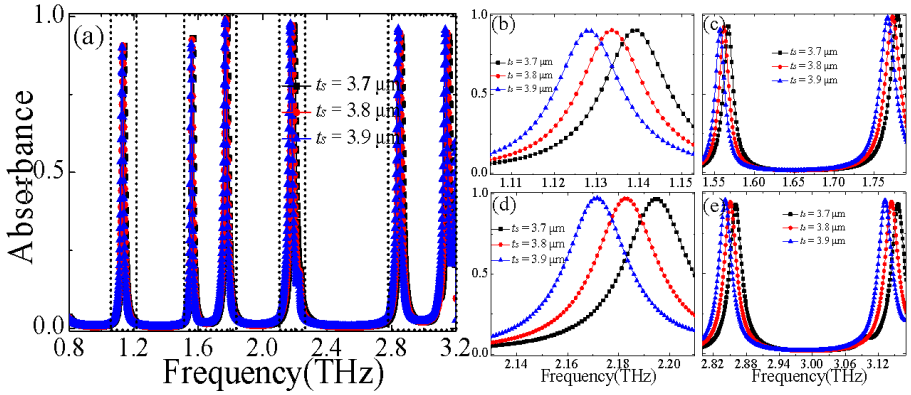

Fig.8. (a) Dependence of the absorption spectra of the proposed PMMA on the size changes of the dielectric layer thickness t_s (t_s = 3.7 μm, 3.8 μm, 3.9 μm), (b-e) the dependence of the absorbance spectra on the t_s under different frequency domain.

Furthermore, we discuss the effect of dielectric layer thickness t_s on the absorption, and Fig.8 shows the calculated absorbance of the PMMA with different dielectric layer thickness t_s (t_s = 3.7 μm, 3.8 μm, 3.9 μm) while the other geometric parameters unchanged. From the Figs.8 (b-d), it is obviously seen that the resonance absorption frequencies (f_1, f_2, f_3, and f_4) drift to the lower frequency and the absorption peak remains unchanged with high level when changing the parameter t_s from 3.7 μm to 3.9 μm. Although the absorption frequencies (f_5 and f_6) also shift to the higher frequency, the absorption peak will decrease with the increase of the dielectric layer thickness t_s as shown in Fig.8 (e).

Based on the above calculation analysis, the absorption peaks and frequencies are sensitive to the geometrical parameters of the unit cell. We could adjust the absorption peaks and frequencies by changing these parameters. Although all changes of the parameters almost affect the shift of the resonant frequency absorption peak, the

designed PMMA still remains high absorption level ($A(\omega) > 90\%$) at resonance. These results further confirm that the frequencies of the designed six-band PMMA could be met different application needs, especially in sensor.

4 Conclusions

In summary, we present an ultrathin six-peak PMMA based on the metallic square cross-cave patch structure placed over a ground plane by a dielectric substrate. Simulations confirm that the absorption peak of the PMMA is more than 95% on average at six different resonance frequencies. The designed PMMA also exhibits a higher Q-factor with more than 65 due to the ultra-narrow-band resonance absorption of the structure. Moreover, the absorption level of designed PMMA can be kept nearly unchanged under different polarization angles for both TE and TM waves. The resonance absorption mechanism of this design is illustrated by studying the electric field distributions at six resonant frequencies. The electric field distributions for different frequencies (f_1, f_2…f_6) reveal that the high level absorption originates from the higher order multipolar plasmon resonance response of the square cross-cave patch structure. Furthermore, the resonance absorption of our design can be tunable by varying the geometric parameters of the unit cell, which gives a considerable freedom to shift or change the operation frequencies of the PMMA to meet different application needs. The simple and efficient design of the six-band PMMA may find numerous potential applications, such as thermal imaging, wavelength selective radiator, thermal bolometer, and biosensor and so on.

ACKNOWLEDGMENT

This work was supported by the National Natural Science Foundation of China (Grant Nos. U1435209, and 61605147) and the Youth science and technology backbone cultivation plan project of the Wuhan University of Science and Technology (Grant No. 2016xz010).

References

[1] N. I. Landy, S. Sajuyigbe, J. J. Mock, D. R. Smith, W. J. Padilla, “Perfect metamaterial absorber,” Phys. Rev. Lett., vol. 100, no. 20, p. 207402, 2008.

Peer-reviewed version available at Materials 2017, 10, 591; doi:10.3390/ma10060591

[2] Y. Z. Cheng, H. L. Yang, Z. Z. Cheng, N. Wu, "Perfect metamaterial absorber based on a split-ring-cross resonator," Appl. Phys. A, vol. 102, pp. 99-103, 2011
[3] Z. W. Mao, S. L. Liu, B. R. Bian, B. Y. Wang, B. Ma, L. Chen, J. Xu, "Multi-Band polarization insensitive metamaterial absorber based on chinese ancient coin-shaped structures," J. Appl. Phys., vol. 115, no.20, p.204505, 2014
[4] Q. Y. Wen, W. Z. Hua, Y. S. Xie, Y. Q. Hu, L. Y. Li, "Dual band terahertz metamaterial absorber: Design, fabrication, and characterization," Appl. Phys. Lett., vol. 95, no. 24, p.241111, 2009
[5] Y. Q. Ye, Y. Jin, S. He, "Omnidirectional, polarization-insensitive and broadband thin absorber in the terahertz regime," J. Opt. Soc. Am. B, vol. 27, no.3, pp.498-504, 2010.
[6] Y. Ma, Q. Chen, J. Grant, S. C. Saha, A. Khalid, D. R. S. Cumming, "A terahertz polarization insensitive dual band metamaterial absorber," Opt. Lett., vol. 36, no. 6, pp. 945-947, 2011.
[7] Y. Z. Cheng, Y. Nie, R. Z. Gong, "A polarization-insensitive and omnidirectional broadband terahertz metamaterial absorber based on coplanar multi-squares films," Opt. Laser Technol., vol.48, no.6, pp. 415-421, 2013.
[8] B. X. Wang, X. Zhai, G. Z. Wang, W. Q. Huang, L. L. Wang, "Design of a four-band and polarization insensitive terahertz metamaterial absorber," IEEE Photonics Journal, vol. 115, no.4, pp.1-8, 2015.
[9] Y. Peng, X. F. Zang, Y. M. Zhu, C. Shi, L. Chen, B. Cai, S. Zhuang, "Ultra-broadband terahertz perfect absorber by exciting multi-order diffractions in a double-layered grating structure," Opt Express, vol. 23, no.3, pp. 2032-2039, 2015.
[10] Y. Z. Cheng, W. Withayachumnankul, A. Upadhyay, D. Headland, Y. Nie, R. Z. Gong, M. Bhaskaran, S. Sriram, D. Abbott, "Ultrabroadband plasmonic absorber for terahertz waves," Advanced Optical Materials, vol.3, pp. 376-380, 2015.
[11] D. Hu, H. Y. Wang, Q. F. Zhu, "Design of six-band terahertz perfect absorber using a simple U-shaped closed-ring resonator," IEEE Photonics Journal vol. 8, no.2, p.5500608, 2016
[12] X. Liu, T. Starr, A. F. Starr, W. J. Padilla, "Infrared spatial and frequency selective metamaterial with near-unity absorbance," Phys. Rev. Lett., vol. 104, no. 20, pp. 207403, 2010.
[13] S. Chen, H. Cheng, H. Yang, J. Li, X. Duan, C. Gu, J. Tian, "Polarization insensitive and omnidirectional broadband near perfect planar metamaterial absorber in the near infrared regime," Appl. Phys. Lett., vol. 99, no. 25, pp. 253104, 2011.
[14] W. Ma, Y. Z. Wen, X. M. Yu, "Broadband metamaterial absorber at mid-infrared using multiplexed cross resonators," Optics Express, vol. 21, no.25, pp. 30724-30730, 2013.
[15] D. Xiao, K. Y. Tao, Q. Wang, "Ultrabroadband mid-infrared light absorption based on a multi-cavity plasmonic metamaterial array," Plasmonics, vol. 11, no.2, pp. 389-394, 2016.
[16] Y. Z. Cheng, X. S. Mao, C. J. Wu, L. Wu, R. Z. Gong, "Infrared non-planar plasmonic perfect absorber for enhanced sensitive refractive index sensing," Optical Materials, vol. 53, no.1, pp.195-200, 2016

[17] Y. Wang, T. Sun, T. Paudel, Y. Zhang, Z. Ren, K. Kempa, "Metamaterial plasmonic absorber structure for high efficiency amorphous silicon solar cells," Nano. Lett., vol. 12, pp. 440-445, 2012.

[18] X. Y. Duan, S. Q. Chen, W. W. Liu, H. Cheng, Z. C. Li, J. G. Tian, "Polarization-insensitive and wide-angle broadband nearly perfect absorber by tunable planar metamaterials in the visible regime," J. Opt., vol. 16, no.14, pp. 125107, 2014

[19] T. Cao, C. Wei, R. E. Simpson, L. Zhang, M. J. Cryam, "Broadband polarization-independent perfect absorber using a phase-change metamaterial at visible frequencies," Sci. Rep., vol. 4, no.2, pp. 3955, 2014.

[20] J. W. Cong, Z. Q. Zhou, B. F. Yun, L. Lv, H. B. Yao, Y. H. Fu, N. F. Ren, "Broadband visible-light absorber via hybridization of propagating surface plasmon," Optics Letters, vol. 41, no.9, pp.1965-1968, 2016.

[21] K. Aydin, V. E. Ferry, R. M. Briggs, H. A. Atwater, "Broadband polarization-independent resonant light absorption using ultrathin plasmonic super absorbers," Nat. Commun., vol. 2, no.517, pp. 1-7, 2011.

[22] J. J. Greffet, R. Carminati, K. Joulain, J. P. Mulet, S. Mainguy, Y. Chen, "Coherent emission of light by thermal sources," Nature, vol. 416, no.6876, pp.61, 2002.

[23] L. Y. Li, J. Wang, H. L. Du, J. F. Wang, S. B. Qu, "Achieving a multiband metamaterial perfect absorber via a hexagonal ring dielectric resonator," Chin. Phys. B vol. 24, no.6, pp. 064201, 2015.

[24] S. J. Li, J. Gao, X. Y. Cao, G. Zheng, "Polarization-insensitive and thin stereometamaterial with broadband angular absorption for the oblique incidence," Appl. Phys. A, vol. 119, pp. 371-378, 2015.

[25] B. M. Adomanis, C. M. Watts, M. Koirala, X. L. Liu, T. Tyler, K. G. West, T. Starr, J. N. Bringuier, A. F. Starr, N. M. Jokerst, W. J. Padilla, "Bilayer metamaterials as fully functional near-perfect infrared absorbers," Appl. Phys. Lett., vol.107, no.2, pp.021107, 2015.

[26] F. Ding, Y. Cui, X. Ge, F. Zhang, Y. Jin, S. He, "Ultra-broadband microwave metamaterial absorber," Appl. Phys. Lett, vol. 100, no.10, pp.103506, 2012.

[27] Y. Z. Cheng, Y. Nie, R. Z. Gong, "Metamaterial absorber and extending absorbance bandwidth based on multi-cross resonators," Appl. Phys. B, vol. 111, no.3, pp. 483-488, 2013.

[28] T. M. Kollatou, A. I. Dimitriadis, S. D. Assimonis, N. V. Kantartzis, C. S, Antonopoulosm, "Multi-band, highly absorbing, microwave metamaterial structures," Appl. Phys. A, vol.115, no. 2, pp. 555-561, 2014.

[29] Y. Cui, K. H. Fuang, J. Xu, H. Ma, Y. Jin, S. He, N. X. Fang, "Ultrabroadband light absorption by a sawtooh anisotropic metamaterial slab," Nano. Lett., vol. 12, no.3, pp. 1443-1447, 2012.

[30] G. Dayal, S. A. Ramakrishna, "Multipolar localized resonances for multi-band metamaterial perfect absorbers," J. Opt., vol.16, p.094016, 2014.

[31] N. V. Dung, P. V. Tuong, Y. J. Yoo, Y. J. Kim, B. S. Tung, V. D. Lam, J. Y. Rhee, K. W. Kim, Y. H. Kim, L. Y. Chen, Y. P. Lee, "Perfect and Broad Absorption by the

Active Control of Electric Resonance in Metamaterial," J. Opt., vol.17, no.4, p.045105, 2015.

[32] B. X. Wang, "Quad-band terahertz metamaterial absorber based on the combining of the dipole and quadrupole resonances of two SRRs," IEEE Journal of Selected Topics in Quantum Electronics, vol. 23, no. 4, p. 4700107, 2017.

[33] N. Liu, S. Kaiser, H. Giessen, "Magnetoinductive and electroinductive coupling in plasmonic metamaterial molecules," Adv. Mater., vol. 20, no. 23, pp. 4521-4525, 2008.

[34] O. P. Gonzalez, N. Zabala, A. G. Borisov, N. J. Halas, P. Nordlander, J. Aizpurua, "Optical spectroscopy of conductive junctions in plasmonic cavities," Nano. Lett., vol.10, no.8, p. 3090, 2010.

[35] X. Shen, T. J. Cui, "Photoexcited broadband redshift switch and strength modulation of terahertz metamaterial absorber," J. Opt., vol.14, no.11, pp.114012, 2012.

[36] Y. Z. Cheng, R. Z. Gong, Z. Z. Cheng, "A photoexcited broadband switchable metamaterial absorber with polarization-insensitive and wide-angle absorption for terahertz waves," Optics Communications, vol. 361, pp. 41-46, 2016.

[37] Z. Liao, Y. Luo, A. I. Fernández-Domínguez, X. P. Shen, S. A. Maier, T. J. Cui, "High-order localized spoof surface plasmon resonances and experimental verifications," Sci. Rep., vol. 5, p.9590, 2015.